

# Interaction of Reactive Gas Flows and Ceramics at High Temperature – Experimental Methods for the Measurement of Species Recombination during Planetary Entry

**Marianne BALAT-PICHELIN**

Laboratoire Procédés, Matériaux et Energie Solaire, PROMES-CNRS, UPR 8521  
rue du four solaire  
66120 Font-Romeu Odeillo  
France  
Tél : +33 468 307 768  
Fax : +33 468 302 940  
[balat@promes.cnrs.fr](mailto:balat@promes.cnrs.fr)

## 1. INTRODUCTION

During the atmospheric re-entry phase of aerospace vehicles, several physico-chemical phenomena taking place on the hot parts (nose cap and wing leading edges) can lead to an important excess of heating and a possible damage of the protective materials.

PROMES-CNRS laboratory has developed since several years experimental methods to study oxidation and catalytic recombination of atomic oxygen under conditions of atmospheric re-entry on Earth and on Mars. The most important conditions for the ground simulation of re-entry (high temperature, low pressure plasma...) have been realized in the MESOX set-up associating a reactor placed at the focus of a solar radiation concentrator and a microwave generator. Concerning the dynamic contribution, only low enthalpy flow can be reproduced on this set-up.

A multi-scale experimental and theoretical approach has been developed to evaluate the recombination parameters.

On one hand, the study of the atomic oxygen recombination on partially catalytic based -silicon or -aluminum ceramic materials, at high temperature (850-2000 K) has been done at different pressures (200-2000 Pa) by a thermal approach, *at a mesoscopic scale* and leads to the determination of the thermal flux of recombination transferred to the material and to the chemical energy accommodation coefficient  $\beta$ . Influences of total pressure, surface temperature and material microstructure are studied.

On the other hand, a chemical approach, *at a microscopic scale* is developed for the evaluation of the recombination coefficient  $\gamma$  using optical emission spectroscopy and actinometry technique on the same device. The values obtained by this method are complementary of the ones of the thermal approach.

*At the atomic scale*, a simulation by Molecular Dynamics is performed in collaboration with Cacciatore from IMIP-CNR, Bari in order to predict atomic oxygen recombination process over silica-based ceramics at high temperatures.

These last decades, the development of thermal protection materials for aerospace vehicles needs surface flux calculations during atmospheric re-entry to predict heat rates. Most of the experiments were realized

on arc-jet plasma facilities where the recombination is obtained from stagnation point heat flux measurement in dissociated flow. The relative heating rates of a known catalytic sample are compared to the surface being studied [1-10].

Some evaluation of catalytic recombination is also obtained by measurement of atom concentration by several techniques (LIF, spectroscopy...) to reach the recombination coefficient  $\gamma$  [11-13]. Other authors have proposed models for recombination and compared to experimental values [2, 4, 14, 15].

Another coefficient  $\beta$  called chemical energy accommodation coefficient is rarely evaluated and often its value is taken equal to 1 (total accommodation). Some authors have tried to measure  $\beta$  and the result is often far from 1 [16-20]. This coefficient is very important because it allows to take into account the real energy transferred to the surface.

In many times, both measurements of flux and  $\gamma$  coefficient to study recombination process are not realized on the same experiment. More often, the flux is measured and the recombination coefficient  $\gamma$  is obtained by calculation. The experimental set-up MESOX that we have developed in our laboratory allows to measure simultaneously the thermal and chemical contributions of the atomic oxygen recombination on surfaces at high temperatures, on the same set-up so the accuracy could be better.

## **2. SURFACE REACTIONS**

### **2.1 Various aspects of dynamics of surface reactions**

Catalysis concerns the rate of a chemical reaction, it is a dynamic phenomenon. A heterogeneously catalyzed reaction consists of a sequence of elementary steps such as adsorption, surface diffusion, chemical transformation of adsorbed species and desorption, needing the identification and characterization of the reaction mechanisms and the transport processes.

The efficiency of a catalyst can be determined by the *macroscopic kinetics* of the overall reaction, including chemical transformations and physical processes of energy and mass transport. The resulting yield depends on external parameters such as temperature, flow rates, partial pressures of the species participating in the reaction. Modelling of the macroscopic kinetics is often achieved by fitting empirical equations, for example using exponential dependent temperature laws (Arrhenius) leading to apparent activation energies as parameters.

The development of sophisticated surface physical methods enabled detailed insights into the atomic processes on surface as well as identification and characterization of the properties of the surface species. Description of the progress of a catalytic reaction in an approach called *microkinetics* is achieved by modelling the macroscopic kinetics through correlating the atomic processes with the macroscopic parameters in the framework of a suitable continuum model. Even if the assumptions underlying a specific continuum model are not completely fulfilled, the model may nevertheless provide a good approximation over a limited range of external parameters. The formulation of the rate laws can lead to a set of nonlinear coupled differential equations for the concentrations of the various species involved at the surface. The resulting temporal behaviour under constant continuous-flow conditions will not be necessarily stationary. Either, the spatial distributions may not be uniform, and the existence of local variations in surface coverage causes coupling of the reaction with adsorbate diffusion or heat transfer processes. So, the formation of spatio-temporal concentration patterns on a *mesoscopic scale* may occur.

The occurrence of interactions between the adsorbed species and their occupation of non equivalent adsorption sites complicates an appropriate description, apart from the fact that the surface is non-uniform and it may undergo structural transformations under the influence of the adsorbates (oxidation,

degradation...). Detailed investigation of these effects on an *atomic scale* represents the classical domain of surface science.

The basic idea of the transition state theory consists of the assumption that at all stages along the reaction coordinate thermal equilibrium is established, leading to the temperature as the only essential parameter. This assumption requires that energy exchange between the degrees of freedom of the particles interacting with the surface and the heat bath of solid occurs much faster than the elementary step initiating nuclear motion. Processes of energy transfer between the various degrees of freedom on the *quantum level* form the ultimate basis for chemical reactions.

## 2.2 Definition of the recombination parameters

The fraction of the chemical energy transferred to the surface by atom recombination depends on the rate at which atoms are recombining and releasing their dissociation energy on the surface.

Four parameters can describe the global recombination reaction:

$\gamma$  : the recombination coefficient, defined as the ratio of the number of recombined atoms to the total number of atoms impinging the surface  $\gamma = [O]_{rec}/[O]_{tot}$

$\beta$  : the chemical energy accommodation coefficient, defined as the ratio of the chemical energy transferred to the surface by recombination to the total energy due to the recombination of atoms.

These two coefficients are comprised between 0 (no recombination, no energy transferred to the surface) and 1 (total recombination or total energy transferred to the surface). The product ( $\gamma \cdot \beta$ ) is often called the effective recombination coefficient  $\gamma$ .

$q_{rec,acc}$  : the thermal flux due to the recombination of species at the surface, linked to the  $\gamma$  coefficient

$k_w$  : the catalytic recombination rate linked to  $\gamma$  by the relation

$$k_w = \gamma \sqrt{\frac{k_B \cdot T}{2\pi M}} \quad (1)$$

## 2.3 Mechanisms of recombination: L-H and E-R

The catalytic recombination process can be divided into main three steps:

- *Adsorption* : 2 types of adsorption are distinguished, physical adsorption (physisorption) where the atom is held to the surface by Van der Waals forces and chemical adsorption, where the bond between atom and surface is of chemical nature (Lennard-Jones potential). In atmospheric re-entry conditions, the temperature of the surface is too high for significant physisorption to take place, which leaves only chemisorption as the mechanism through which catalytic recombination can occur ;
- *Recombination* : Here too, 2 types are considered. In the first, two adhered atoms, located at adjacent sites combine to form a molecule (*Langmuir-Hinshelwood mechanism*) and in the second, recombination occurs when a gas-phase atom collides with a surface-adhered atom (*Eley-Rideal mechanism*).
- *Desorption* : The final step in catalytic recombination is the desorption of the recombined molecule from the surface, leaving the site it occupied for new atom adsorption.

At low temperatures, the L-H mechanism seems favourable to the E-R mechanism, because of the high surface coverage. For high temperatures, the thermal agitation of adsorbed atoms becomes more important, and the fraction of surface sites occupied, is expected to drop. Therefore, unless the mobility of atoms adsorbed at the surface is high, the L-H mechanism will not play an important role in the catalytic recombination process. Highly mobile adhered surface atoms are an unlikely phenomenon, because of the nature of the adsorption. Furthermore, in most experiments, catalytic recombination is found to be a first order reaction, indicating that the E-R mechanism is dominant in the reaction process.

### **3. EXPERIMENTAL SET-UP MESOX**

The MESOX set-up (Moyen d'Essai Solaire d'OXYdation) that associates a quartz tube reactor placed at the focus of the 6 kW solar radiation concentrator for sample heating (up to 2500 K under pressures comprised between  $10^2$  and  $10^5$  Pa) and a microwave generator (2450 MHz, 1200 W max) is presented on Figure 1. Originally developed for oxidation studies, it has been adapted to allow atomic recombination measurements. Atmospheric entry conditions can be partially simulated, pressure and temperature can be reproduced independently with a high accuracy.

The experimental device is placed at the focus of a solar furnace equipped with a variable opening shutter. It can be moved away from the focus to be replaced by a calorimeter to measure the incident concentrated solar flux that can reach  $5 \text{ MW.m}^2$ . The temperature measurements on front and back faces of the sample are realized using a single optical pyrometer ( $5 \mu\text{m}$ ) with a system of one rotating mirror and two stationary mirrors. The experimental reactor consists of a quartz tube, 50 cm length and 5 cm diameter with  $\text{CaF}_2$  viewports. This reactor crossing the refrigerated waveguide contains the sample (25 mm diameter and 3 mm height) placed in stagnation point position at the center of the discharge. A regulator, a gauge and a vacuum pump are used to control precisely the total pressure during the experiment.

The spectroscopic bench is composed of an optical sampling system including a lens and a mirror, and a monochromator (spectrometer Triax 550 Jobin-Yvon) equipped with an Optical Multichannel Analyzer (OMA). The microwave discharge is imaged by the silica lens (magnification 0.1) on the slit entrance of the monochromator. The 55 cm focal length monochromator working with a 1200 grooves/mm grating (also available 1800 and 2400 grooves/mm gratings) and a  $100 \mu\text{m}$  width slit allows a spectral resolution of 0.2 nm. The dispersed light is analyzed by means of the CCD matrix (1024 x 128) of the OMA detector. Each of the 128 lines of the matrix gives information on the relative atomic oxygen concentration at different distances from the surface of the sample with a spatial resolution around  $270 \mu\text{m}$ . A spectral analysis over the 128 lines is performed very quickly after the solar radiation breaking. The total duration of a scan is 200 ms. Therefore, all the spectral and spatial needed informations are taken simultaneously allowing a good accuracy.

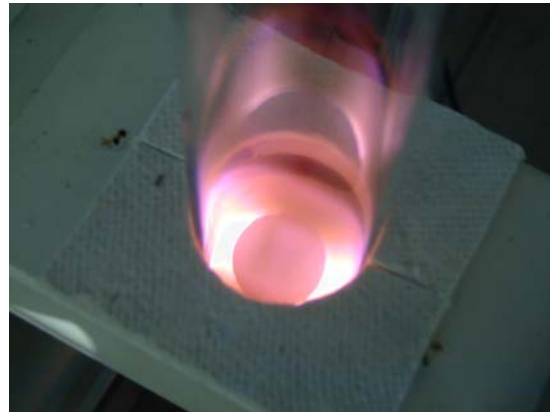
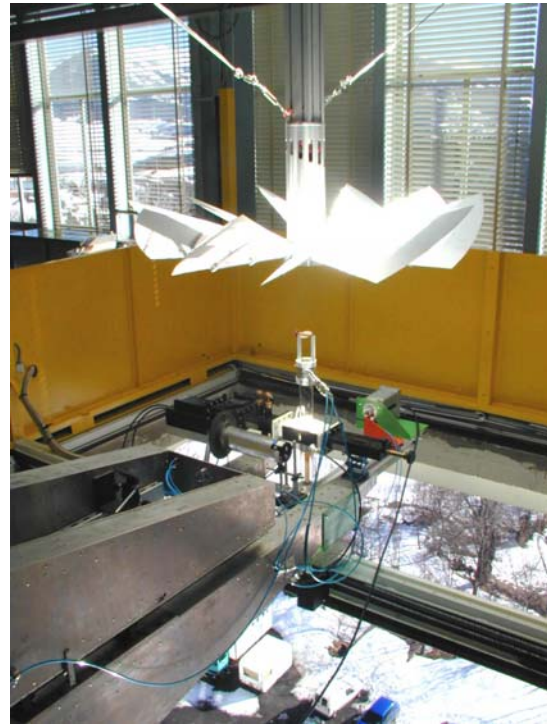


Figure 1: Experimental set-up MESOX with the irradiated shutter (top, right) placed at the focus of the 6 kW solar furnace (top, left). Images of plasma environment: CO<sub>2</sub> (down, left) and air (down, right).

## 4. EXPERIMENTAL DETERMINATION OF THE RECOMBINATION OF ATOMIC OXYGEN AT HIGH TEMPERATURE

In this chapter, the presentation of the experimental methods developed for the evaluation of recombination parameters is carried out according to a multi-scale approach.

### 4.1 Mesoscopic approach: thermal flux of recombination

A mesoscopic approach for the evaluation of the atomic oxygen recombination has been developed using a thermal balance done on a reference cylinder volume in the sample. The surface of this cylinder of 6 mm diameter and 3 mm height in the sample, considered for the thermal balance (Fig. 2), represents the measurement area by pyrometry. Convective phenomena are neglected (rarefied gas flows) compared to the radiative fluxes to establish the equations for steady state heat transfer under different environments. The thermal balance is established under each atmosphere: standard air, air plasma, standard argon and argon plasma, the determination of the recombination flux being done by difference between the experiments under air plasma (reactive) and argon plasma (inert).

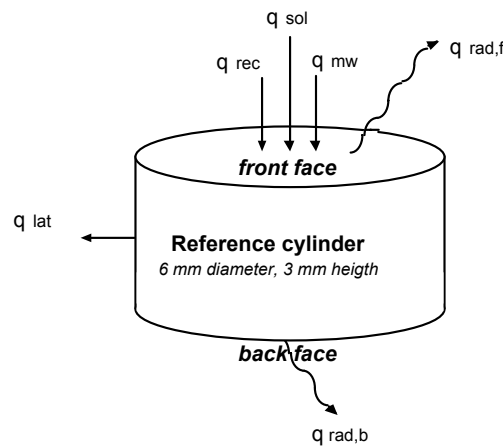


Figure 2: Reference cylinder considered for the evaluation of the thermal flux of recombination under air plasma conditions

*Under standard air:* the sample is heated only by solar radiation

$$\alpha \cdot q_{\text{sol}}^{\text{air}} = q_{\text{rad},f}^{\text{air}} + q_{\text{rad},b}^{\text{air}} + q_{\text{lat}}^{\text{air}} \quad (2)$$

*Under air plasma:* the sample is heated by solar radiation, by microwave-material interaction and by atomic oxygen recombination

$$\alpha \cdot q_{\text{sol}}^{\text{air},*} + q_{\text{mw}}^{\text{air},*} + q_{\text{rec,acc}}^{\text{air},*} = q_{\text{rad},f}^{\text{air},*} + q_{\text{rad},b}^{\text{air},*} + q_{\text{lat}}^{\text{air},*} \quad (3)$$

*Under standard argon:* the sample is heated only by solar radiation, like in standard air

$$\alpha \cdot q_{\text{sol}}^{\text{arg}} = q_{\text{rad},f}^{\text{arg}} + q_{\text{rad},b}^{\text{arg}} + q_{\text{lat}}^{\text{arg}} \quad (4)$$

*Under argon plasma:* the sample is heated by solar radiation and by microwave-material interaction

$$\alpha \cdot q_{\text{sol}}^{\text{arg},*} + q_{\text{mw}}^{\text{arg},*} = q_{\text{rad},f}^{\text{arg},*} + q_{\text{rad},b}^{\text{arg},*} + q_{\text{lat}}^{\text{arg},*} \quad (5)$$

The thermal flux of recombination is obtained by difference between Eq. (3) and (5), and we can neglect the difference between the radial losses by conduction out of the reference cylinder because the radial losses are of same order in air and argon plasmas.

Under the following assumptions (some are experimentally verified) a like-one dimensional equation is obtained:

- without plasma, the same temperature level is reached for both air and argon atmospheres, that is  $T_f^{\text{air}} = T_f^{\text{arg}}$  and  $T_b^{\text{air}} = T_b^{\text{arg}}$ ; this is due to the constant solar flux, experiments being done around the period of solar zenith;

- under plasma, the microwave-material interaction for both the atmospheres is supposed equal so  $q_{\text{mw}}^{\text{air},*} = q_{\text{mw}}^{\text{arg},*}$ ; this will be verified when the dielectric permittivity of the samples tested may be measured at high temperature and so the absorbed power may be known;

- the absorbed solar energy is constant under the different atmospheres for a given shutter opening because during all the experiment the incident solar flux is constant;

- the radial losses by conduction out of the reference cylinder are neglected. Infrared imaging on the front face of the sample has allowed to determine a weak radial temperature gradient as function of distance from the centre, even when the sample is heated under air or argon plasma.

So, the thermal balance is reduced to a 1D approach. Finally, it comes

$$q_{\text{rec,acc}}^{\text{air},*} = q_{\text{rad,f}}^{\text{air},*} - q_{\text{rad,f}}^{\text{arg},*} + q_{\text{rad,b}}^{\text{air},*} - q_{\text{rad,b}}^{\text{arg},*} \quad (6)$$

equivalent to :

$$q_{\text{rec,acc}}^{\text{air},*} = \varepsilon \sigma [(T_f^{\text{air},*})^4 - (T_f^{\text{arg},*})^4 + (T_b^{\text{air},*})^4 - (T_b^{\text{arg},*})^4] \quad (7)$$

The thermal flux of recombination transferred to the surface can be calculated from the following parameters:  $\varepsilon$  the total hemispherical emissivity and  $T_f^*$  and  $T_b^*$  the front and back face temperatures under air and argon plasmas.

The uncertainties  $\Delta q_{\text{rec,acc}}/q_{\text{rec,acc}}$  have been calculated taking into account the errors on temperature measurements due to the accuracy of the optical pyrometer (0.5%), on the spectral emissivity (at 5  $\mu\text{m}$ , 1 to 2% depending on the materials) and on the total hemispherical emissivity (1%). The emissivity measurements are done in our laboratory by a direct method using a two-color (1.3 and 1.55  $\mu\text{m}$ ) pyrometer for the temperature measurement and a spectroradiometer for the radiance determination [21]. The accuracy is mentioned on Table 2 but not on Figure 3 for a better visualization of the experimental points.

#### 4.1.1 Experimental results

The pressure and the flow rate ( $10^{-6} \text{ m}^3 \cdot \text{s}^{-1}$ ) are fixed at the beginning of each experiment. Three total gas pressures have been applied: 200, 1000 and 2000 Pa, for five temperature levels (1000, 1200, 1400, 1600 and 1800 K). The surface temperature depends on the incident solar flux controlled by the opening of the shutter.

The study has been realized on sintered materials (SiC,  $\text{Si}_3\text{N}_4$ , AlN,  $\text{Al}_2\text{O}_3$ ) or on samples obtained by oxidation at 1300 K under atmospheric pressure during 24 hours (SiC +  $\text{SiO}_2$ , AlN +  $\text{Al}_2\text{O}_3$ ).

Table 2 shows the temperature increase due to the atomic oxygen recombination on the surface of different materials deduced from the difference under air and argon plasmas at 2000 and 200 Pa according to the relation:

$$\Delta T_f = T_f^{\text{air,*}} - T_f^{\text{air}} - (T_f^{\text{arg,*}} - T_f^{\text{arg}}) \quad (8)$$

The temperature increase due to the catalytic recombination for all the tested materials decreases rapidly with temperature. The silicon-based ceramics have weaker  $\Delta T_f$  than the aluminum ones and particularly than the sintered alumina ( $\Delta T_f = 350$  K at 1000 K).

A graphical representation of the results for the thermal fluxes of recombination obtained from Eq. (7) is shown on Figure 3 for some materials tested at 2000 and 200 Pa, at five temperature levels.

The determination of the thermal flux of recombination confirms the tendencies obtained with the temperature increase. Silicon-based ceramic materials have similar and low catalytic activities. The sintered SiC has the weakest recombination flux (at 200 Pa) that is nearly constant between 1000 and 1600 K (around  $30 \text{ kW}\cdot\text{m}^{-2}$ ), except under active oxidation [22], at 1800 K ( $13 \text{ kW}\cdot\text{m}^{-2}$ ). This confirms its very low catalytic activity, the higher values obtained between 1000 and 1600 K being due to the presence of a thin silica layer formed during experiment, like in the case at 2000 Pa (see Table 2). Aluminum-based ceramic materials have more pronounced catalytic activities and sintered alumina is by far the more catalytic material with an increasing recombination flux that reaches  $151 \text{ kW}\cdot\text{m}^{-2}$  at 1400 K for 200 Pa and  $184 \text{ kW}\cdot\text{m}^{-2}$  at 2000 Pa, before decreasing at 1800 K (respectively  $65 \text{ kW}\cdot\text{m}^{-2}$  at 200 Pa and  $93 \text{ kW}\cdot\text{m}^{-2}$  at 2000 Pa). Here, on Table 2, we can see the influence of the total pressure: higher total pressures lead to higher thermal flux of recombination.

<i>Sintered SiC 2000 Pa</i>			<i>Sintered AlN + Al<sub>2</sub>O<sub>3</sub></i>			<i>Sintered Al<sub>2</sub>O<sub>3</sub></i>		
T <sub>f</sub> (K)	ΔT <sub>f</sub>	q <sub>rec,acc</sub> <sup>1D/2D</sup> (kW/m <sup>2</sup> )	T <sub>f</sub> (K)	ΔT <sub>f</sub>	q <sub>rec,acc</sub> <sup>1D</sup> (kW/m <sup>2</sup> )	T <sub>f</sub> (K)	ΔT <sub>f</sub>	q <sub>rec,acc</sub> <sup>1D/2D</sup> (kW/m <sup>2</sup> )
984±3	74	37±3 / 43	994±6	125	58±8	982±6	354	136±22 / 154
1196±5	45	35±3 / 40	1174±10	94	59±9	1173±9	301	149±27 / 168
1386±7	30	33±3 / 38	1409±14	52	48±9	1364±11	304	184±37 / 202
1598±9	21	34±3 / 36	1572±17	40	48±9	1597±16	154	113±25 / 126
1775±11	19	36±4 / 40	1769±21	28	42±9	1767±21	107	93±23 / 106

<i>Sintered SiC 200 Pa</i>			<i>Sintered AlN + Al<sub>2</sub>O<sub>3</sub></i>			<i>Sintered Al<sub>2</sub>O<sub>3</sub></i>		
T <sub>f</sub> (K)	ΔT <sub>f</sub>	q <sub>rec,acc</sub> <sup>1D/2D</sup> (kW/m <sup>2</sup> )	T <sub>f</sub> (K)	ΔT <sub>f</sub>	q <sub>rec,acc</sub> <sup>1D</sup> (kW/m <sup>2</sup> )	T <sub>f</sub> (K)	ΔT <sub>f</sub>	q <sub>rec,acc</sub> <sup>1D/2D</sup> (kW/m <sup>2</sup> )
984±3	64	30±2 / 34	972±6	113	48±7	975±6	281	97±16 / 109
1191±5	38	29±2 / 31	1179±10	88	56±9	1168±9	287	139±24 / 153
1377±7	27	30±3 / 32	1380±14	55	51±9	1399±11	251	151±29 / 166
1591±9	16	25±2 / 26	1577±17	36	38±7	1577±16	153	108±23 / 120
1780±11	7	13±2 / 15	1771±21	26	34±7	1710±20	81	65±15 / -

**Table 2 : Experimental data for atomic oxygen recombination on ceramic materials at 2000 (top) and 200 (down) Pa where T<sub>f</sub> is the front face temperature, ΔT<sub>f</sub> the front face temperature increase due to the recombination and q<sub>rec,acc</sub> the thermal flux of recombination.**

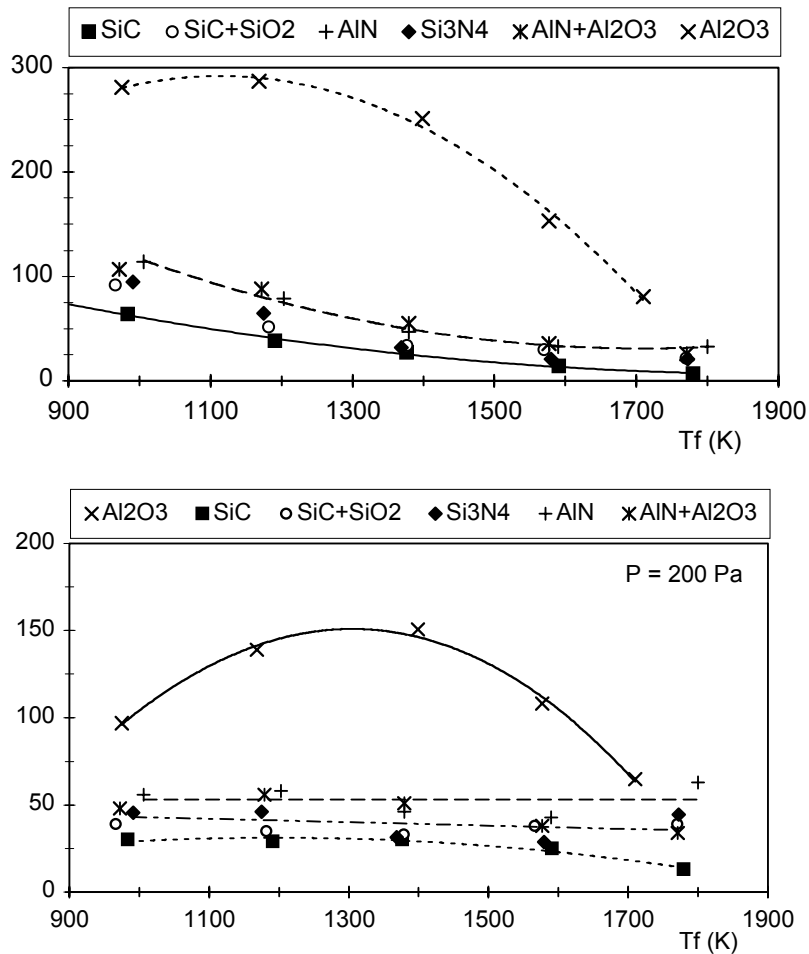


**Figure 3: Increasing in temperature due to recombination (top) and thermal flux of recombination transferred to the surface (down) for some materials under 200 Pa air plasma.**

#### 4.1.2 Comparison of modelling and experimental results

A bi-dimensional model has been developed in order to estimate the radial thermal losses by conduction that have been neglected in the experimental part. This 2-D model is developed in order to estimate the radial thermal losses that have been neglected in equation (7), on the whole sample, and to calculate by parameter identification the thermal flux of recombination. This model is based on the simulation of axial and radial heat transfers in the material at high temperature. The 2-direction heat equation with added source terms (one due to the microwave-material interaction, since the sample is in the electromagnetic field and another one due to the recombination) is solved with a finite difference scheme that is applied to a cylindrical shape. This code is written with Matlab™ and gives a temperature mapping of the sample front face (where recombination occurs) that is compared to camera-obtained infra-red images. The code gives also the sample back face temperature mapping and that of its thickness [23]. A comparison is done between:

- the experimental values of the thermal flux of recombination and the values obtained by modelling ;
- the temperature mapping of the samples obtained by modelling and those experimentally acquired using an infra-red camera.

The problem is solved by using the codes called MAT2D and REC2D. With the material characteristics and the boundary conditions, the codes compute the temperature distribution in the sample (MAT2D) and determine the thermal flux of recombination  $q_{\text{rec,acc}}^{2D}$  (REC2D) which is compared to the experimental value  $q_{\text{rec,acc}}^{1D}$ .

For the determination of the thermal flux of recombination using the code REC2D, several stages are necessary. At each stage, one parameter is identified according to the experimental values of temperature. This parameter is validated when the computed temperatures are equal to the experimental ones. The different stages are the following:

- First, an experiment is done under standard air. The microwave flux absorbed by the sample and the thermal flux of recombination are equal to zero. In this case, the value of the incident solar flux  $q_{\text{sol}}$  is measured using a calorimeter. The only unknown value is the apparent solar absorptivity  $\alpha$ . Its value is assumed to be correct when  $T_{2D}^{\text{air}} = T_{\text{exp}}^{\text{air}}$ , that is to say when the temperature obtained by the modelling and the experiment are equal ;
- Second, an experiment is performed under argon plasma. The thermal flux of recombination is equal to zero. The apparent solar absorptivity is known by the first stage, so the only unknown is, in this case, the microwave flux absorbed by the sample. As previously, its value is supposed to be correct when  $T_{2D}^{\text{arg}^*} = T_{\text{exp}}^{\text{arg}^*}$  under plasma conditions ( $\dot{\cdot}$ ) ;
- The last stage is an experiment under air plasma (reactive gas). The apparent solar absorptivity  $\alpha$  and the microwave flux absorbed by the sample  $q_{\text{mw}}$  are known using the preceding stages, so the only unknown is now the thermal flux of recombination transferred to the surface sample  $q_{\text{rec,acc}}$ . Its value is determined when  $T_{2D}^{\text{air}^*} = T_{\text{exp}}^{\text{air}^*}$  under air plasma conditions ( $\text{air}^*$ ).

The results of the calculations are given in Table 2 for two sintered materials (SiC and  $\text{Al}_2\text{O}_3$ ). Most of the results obtained by the model REC2D are in good agreement with the experimental values taking into account the accuracy of the experimental results. The results obtained for sintered SiC (less catalytic ceramic) and  $\text{Al}_2\text{O}_3$  (highest catalytic ceramic) at 200 and 2000 Pa air, under plasma conditions, are given in Table 2. The values of the thermal flux of recombination obtained by experiment ( $q_{\text{rec,acc}}^{1D}$ ) are very near the calculated ones ( $q_{\text{rec,acc}}^{2D}$ ) thus proving that the hypotheses chosen for the experimental evaluation are valid for the ceramic materials tested. The main hypothesis (difference between both radial losses negligible) appears to be less important at high temperature as shown in Table 2, so the experimental results present a better accuracy at high temperature (1600-1800 K).

#### **4.2 Microscopic approach: recombination coefficient**

The actinometry technique is used to follow the relative atomic oxygen concentration profile along the discharge. A low known quantity of argon is introduced in the flow and the evolution of the intensities ratio  $I_{\text{O}}/I_{\text{Ar}}$  of an oxygen line to an argon line is measured along the discharge zone.

Some assumptions are necessary using actinometry:

- the actinometer must be introduced in low quantity so as not to disturb the plasma ;
- the excited species must be solely produced by electronic impact from the ground state ;
- the desexcitation of the species must be essentially radiative ;
- the energy dependencies of the cross sections of electronic excitation of O and Ar must be identical in theory and, at the least, the energy thresholds of the transition must be similar.

To determine the spatial variation of the relative concentration of atomic oxygen, we use its most reliable transition at 844.6 nm. For the actinometer line, we choose the argon transition at 842.4 nm that presents a similar energy threshold (13.1 eV) than for the atomic oxygen transition (11 eV). Thus, it is reasonable to

assume that the ratio of the intensities of the two lines is proportional to the oxygen atom concentration. Moreover, the lines 842.4 and 844.6 nm can be recorded simultaneously that increasing the accuracy of the intensities ratio measurements [24].

We have chosen to work at a constant microwave power of 300 W, a total air pressure of 200 Pa and a total flow of  $10^{-6} \text{ m}^3 \text{ s}^{-1}$  with 5 % argon. In this type of microwave plasma, as shown by several authors [25-28], the oxygen atom concentration is strongly increased when the amount of nitrogen is increased. Recently, we have used fiber-optics catalytic probe to measure the absolute density of neutral oxygen atoms in our reactor in collaboration with Mozetic and Vesel from the Jozef Stefan Institute (Ljubljana, Slovenia). The degree of the dissociation of oxygen molecules in our 2450 MHz air plasma is around 80% for the above conditions of flow rate (to be published).

A cylindrical volume corresponding to the discharge zone is considered, every point being represented by the coordinates (r, x). As the mean free path of the atoms (0.043 cm at 200 Pa) is less than the diameter of the reactor (5 cm), the atom diffusion is given by the diffusion equation written in cylindrical coordinates that describes the variation of the concentration  $C_O$  of an oxygen atom O versus time for a fixed point in the cylinder (r, x):

$$\frac{\partial C_O}{\partial t} + \text{div} C_O \cdot U_x + \text{div} C_O \cdot U_r + \omega = 0 \quad (9)$$

with  $\omega$  the variation of the concentration due to the recombination in the gaseous phase and on the reactor walls.

In steady state conditions, equation (9) is reduced to:

$$D \cdot \left( \frac{\partial^2 C_O}{\partial x^2} + \frac{\partial^2 C_O}{\partial r^2} + \frac{1}{r} \frac{\partial C_O}{\partial r} \right) + \omega = 0 \quad (10)$$

We suppose that the convective transfer is negligible. The radial gradient in the reactor is negligible compared to the axial one, so the concentration is only function of x. Moreover, the stability of the ratio  $I_O/I_{Ar}$  in the reactor allows neglecting the recombination in volume and on the reactor wall.

Thus, equation (10) can be simplified in:

$$D \cdot \frac{\partial^2 C_O}{\partial x^2} = 0 \quad (11)$$

This equation has two limit conditions:

- the ratio  $I_O/I_{Ar}$  is constant along the discharge, thus, far from the sample, the concentration has a known fixed value :  $C_O(x = L) = \text{constant}$
- at the surface sample ( $x = 0$ ), the mass balance in oxygen atoms is established by the equality between the oxygen arriving at the surface by diffusion and the atomic oxygen recombined at the surface :

$$-D_{O, \text{air}} \cdot \frac{\partial C_O}{\partial x} \Big|_{x=0} - C_O(x=0) \cdot \frac{\gamma \cdot V}{4} = 0 \quad (12)$$

with V the mean square velocity of oxygen atoms.

The evolution of the atomic oxygen concentration is given by the solution of equation (11).

Finally, the intensities ratio obtained by actinometry leads to the determination of the recombination coefficient  $\gamma$  by the following equation:

$$\gamma = \left( \frac{\frac{I_{O}}{I_{Ar}} \Big|_{x=L} \frac{T_S}{T_L} - 1}{\frac{I_{O}}{I_{Ar}} \Big|_{x=0}} \right) \cdot \frac{4 \cdot D_{O,air}}{V \cdot L} \quad (13)$$

with  $I_{O}/I_{Ar}$  the ratio of the intensities respectively at the entrance of the reactor ( $x = L$ ) and at the surface sample ( $x = 0$ ),  $D_{O,air}$  the binary diffusion coefficient of atomic oxygen in air,  $V$  the mean square atomic velocity and  $L$  the thickness of the recombination boundary layer.

#### 4.2.1 Experimental results

The uncertainties  $\Delta\gamma/\gamma$  have been calculated taking into account the errors on  $I_{O}/I_{Ar}$  and  $L$  but also on the flow parameters: the binary diffusion coefficient  $D_{O,air}$  determined using the Chapman-Enskog theory and the mean square atomic velocity  $V$  determined using the gas kinetic theory (rarefied gas). The accuracy on these two last values is due essentially to that of the gas temperature, measured by emission spectroscopy ( $N_2$  rotational temperature), this leading to a total accuracy on  $\gamma_O$  of  $\pm 30\%$ .

For nearly all the materials, after the acquisition of the plasma image, we observe a constant level for the concentration profile of atomic oxygen until 6 mm from the surface leading by a progressive decrease and then, at 1.5 mm from the surface, there is a change in the slope that we consider representative of the recombination phenomena occurring on the material surface.

We have applied the actinometry method on sintered SiC oxidized during the  $\gamma$  measurement in  $SiO_2$   $\beta$ -cristobalite and on  $SiO_2$  quartz, on two sintered alumina and on an alumina layer obtained by oxidation at 1300 K at atmospheric pressure during 24 h on sintered AlN. The values of the recombination coefficient have been calculated for each material with the concentration profile and are given on Figures 4 to 7. Figure 4 presents the results for the two polymorphs of silica, Figure 5 the AFM images of both the silica samples and Figures 6 and 7 the  $\gamma$  results for the three alumina samples different by their impurity content.

##### 4.2.1.1 Silica polymorphs samples

The silica polymorphs samples studied were (i) the silica layer ( $\beta$ -cristobalite) obtained by oxidation on sintered SiC,  $\alpha$ -6H containing less than 1% mass boron and (ii) silica, quartz.

The results presented on Figure 4 show the very weak catalytic activity of quartz. On the contrary, the recombination coefficient of  $SiO_2$   $\beta$ -cristobalite is roughly four times higher [24]. According to Figure 4, the apparent activation energy of recombination  $E_a$  using an Arrhenius law for the recombination coefficient gives:

- for SiO<sub>2</sub> β-cristobalite :  
 $\gamma = 0.6382 \exp(-3374/T)$       and    $E_a = 28.0 \pm 0.6 \text{ kJ/mol}$       between 800 and 1830 K
- for SiO<sub>2</sub> quartz :  
 $\gamma = 0.0622 \exp(-2158/T)$       and    $E_a = 17.9 \pm 0.6 \text{ kJ/mol}$       between 850 and 1430 K

The accuracy on the activation energy values is calculated from several measurements.

For β-cristobalite and quartz, the recombination coefficient increases with temperature, so the mechanism of recombination seems to be the same along the temperature range and probably with a preponderance of the Eley-Rideal mechanism. To determine the main recombination mechanism between the Eley-Rideal and Langmuir-Hinshelwood processes for the recombination of atomic oxygen at high temperatures on these ceramic materials, a study was carried out using Molecular Dynamics Simulation in collaboration with Cacciatore from IMIP-CNR (Bari, Italy) [29-31, also see in this lecture series].

It can also be noticed the importance of the microstructure of the material as far as the crystalline structure and the surface morphology are concerned. Around 1000 K, the recombination coefficients determined experimentally are  $27.10^{-3}$  for β-cristobalite and  $8.10^{-3}$  for quartz. Such a trend is confirmed at higher temperatures (at 1400 K,  $60.10^{-3}$  for β-cristobalite and  $14.10^{-3}$  for quartz). These results confirm the importance of the crystalline structure because, in spite of a greater specific area for quartz than for β-cristobalite as revealed by the micrographs obtained by SEM and AFM (Fig. 5), the catalytic activity is weaker for quartz.

Many models developed to describe the evolution of the recombination coefficient  $\gamma$  with temperature predict a very important decrease of  $\gamma$  at high temperature [2-6, 14, 15]. Figure 4 shows the decreasing of the recombination coefficient around 1800 K. This effect can be attributed:

- to the change in the reaction order : before the “critical temperature” corresponding to the fall-off of the recombination coefficient, the reaction is first order and above this temperature (around 1800 K), the reaction becomes second order with a square dependence on pressure as proposed by Jumper [2] ,
- or to the thermal desorption of atoms that becomes important at high temperature, further reducing the numbers of adsorbed atoms as proposed by several authors [3, 4, 14, 15, 20].

In order to confirm these experimental results and to eventually prove experimentally the decrease of  $\gamma$  after a critical temperature, we have then perform measurements at higher surface temperatures up to 2300 K on refractory oxides such as alumina, because at these temperature levels the alumina surface remains unchanged. Also, further investigations based on AFM characterization to reveal the roughness at a nanometer scale and the possible active sites have to be done for a better understanding of these experimental results on alumina.

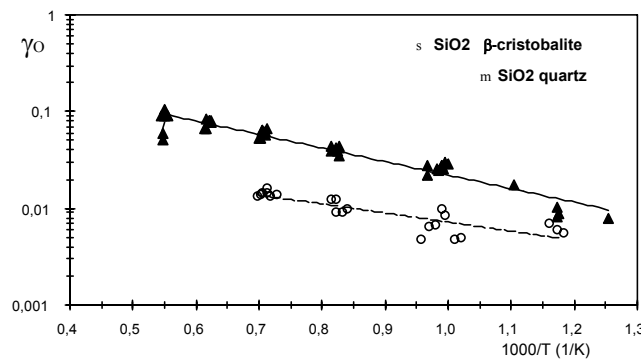


Figure 4: Atomic oxygen recombination coefficient  $\gamma_{\text{O}}$  for SiO<sub>2</sub> β-cristobalite and quartz versus reciprocal temperature

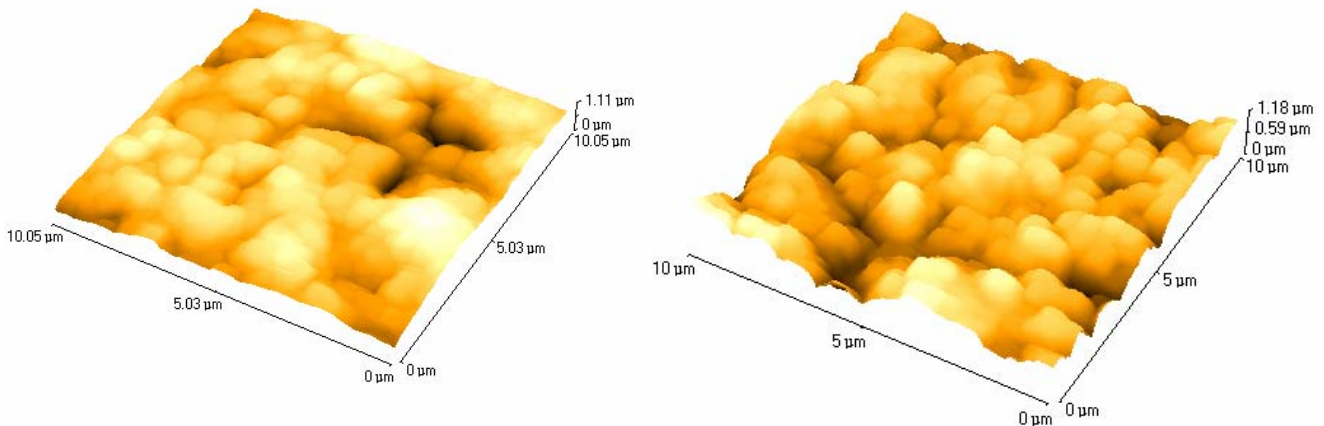


Figure 5: AFM images (10 x 10 μm) for β-cristobalite (left) and quartz (right)

#### 4.2.1.2 Alumina samples

Two sintered alumina called A and B (A for AF 997 Saint-Gobain Céramiques, and B for AluSiK 99 ZA from Anderman Céramiques) and a coating of alumina obtained by oxidation of an AlN sintered material called C (AlN from Saint-Gobain Céramiques) were studied. The two sintered alumina A and B have respectively a purity of 99,7% and 99,8%, a density of 3,9 and 3,8 g/cm<sup>3</sup> and an open porosity equal to zero for both. The AlN material contains around 3 to 5% Y<sub>2</sub>O<sub>3</sub> as a sintering aid and some yttrium is present in the oxide layer as revealed by XRD and XPS analyses.

The choice of these α-alumina samples to study the recombination was made according to the fact that:

- we have previously shown that the crystal lattice is an important parameter to take into account for the catalyticity,  $\beta$ -cristobalite being more catalytic than quartz
- so, we chose an  $\alpha$ - $\text{Al}_2\text{O}_3$  and modify the microstructure of the material by the presence of impurities in low or relative high content to see if it is an influent parameter
- alumina is a high stable refractory oxide, that allows to perform measurement of recombination parameters until very high temperatures with no modification of the material, and also around the melting point (2323 K) to eventually measure the sharp decrease in the curve  $\text{Log } \gamma = f(1/T)$ .

The recombination coefficients  $\gamma$  have been calculated for alumina with the measured concentration profiles, obtained in steady-state conditions, and are plotted on Figures 6 and 7. These results show the strong catalytic activity of alumina if we compare with the previous results obtained on silica (Fig. 4). Hence, in all the temperature range, Arrhenius fits of the experimental dots is still possible. We have to notice that, for both the sintered alumina, around 1400 K, there is a change in the slope of the curves. This was already observed for the measurement of the thermal flux of recombination on the same alumina at the same temperature and was not explained (Fig. 3). Now, we think that probably, there is a change in the recombination mechanism passing from a Langmuir-Hinshelwood reaction (below 1400 K) to an Eley-Rideal one (above 1400 K). This has to be verified using Molecular Dynamics simulation, such as demonstrated by Cacciatore on silica [32]. This is also under study with Guerra using modelling with asymptotic analytic solutions [33].

The following expressions were obtained for  $\gamma$  and the respective apparent activation energies:

- for the A alumina (AF 997):  
 $\gamma = 0.2162 \exp(-1997/T)$  and  $E_a \approx 16 \text{ kJ/mol}$  below 1400 K  
 $\gamma = 25.436 \exp(-8747/T)$  and  $E_a \approx 73 \text{ kJ/mol}$  above 1400 K
- for the B alumina (Anderman):  
 $\gamma = 0.1588 \exp(-1140/T)$  and  $E_a \approx 10 \text{ kJ/mol}$  below 1400 K  
 $\gamma = 3.4788 \exp(-5423/T)$  and  $E_a \approx 45 \text{ kJ/mol}$  above 1400 K to 2030 K  
 $\gamma = 0.26$  in the range 2330-2430 K (fused zone)
- for the C alumina (coating on AlN):  
 $\gamma = 1.896 \exp(-5042/T)$  and  $E_a = 42 \text{ kJ/mol}$  ( $880 \leq T \leq 2000 \text{ K}$ )

The accuracy on the activation values is also calculated from several measurements. The two activation energies obtained for sintered  $\text{Al}_2\text{O}_3$  show that the recombination mechanism may be different for the two temperature ranges around 1400 K. In the thermal study (Fig. 3), this change was also encountered around 1400 K.

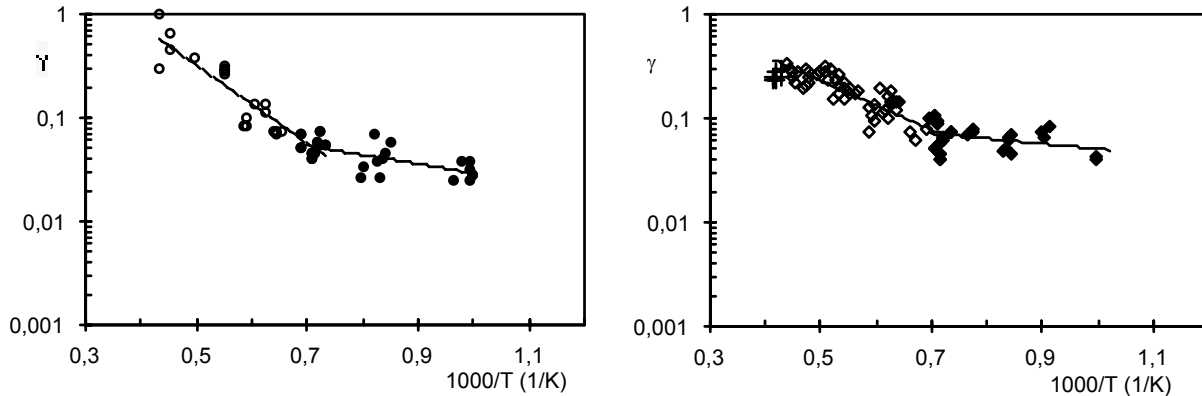


**Figure 6: Atomic oxygen recombination coefficient  $\gamma$  for two sintered alumina samples versus reciprocal temperature: A on the left and B on the right**

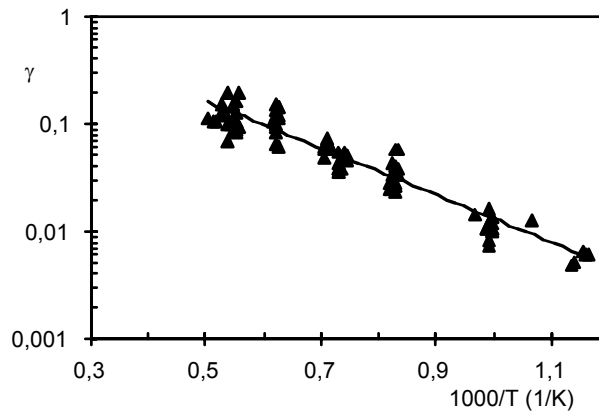


**Figure 7: Atomic oxygen recombination coefficient  $\gamma$  for alumina on AlN versus reciprocal temperature**

X-ray Photoelectron Spectroscopy (XPS) was used to analyze the surfaces of the tested samples after the measurement of the recombination coefficient  $\gamma$  [34]. The alumina coating on AlN (C alumina) is characterized by the presence of a photoelectron peak Y 3d due to the fact that  $Y_2O_3$  is a sintering additive of the AlN material present under the oxide layer of alumina. For this sample, N was not detected proving that the oxide layer is more than 30 nm thick. This oxide layer was formed during a 24 h oxidation at 1300 K under atmospheric pressure in an electrical furnace. A comparison of the Al 2p spectra corresponding to samples C and A was done. A broadening of the Al 2p peak for sample C can be observed in comparison with the one of sample A without yttrium. Therefore, the Al 2p peak of sample C was fitted into two peaks, one located at a binding energy of 74.5 eV corresponding to the Al 2p peak in  $Al_2O_3$  and the other located at 73.3 eV. This last peak can be attributed to one kind of Al present in the garnet YAG phase of composition  $Y_3Al_2(AlO_4)_3$  also detected by XRD, this phase having two different sites for aluminum: one in tetrahedral coordination number (peak at 74.5 eV) and the other in octahedral coordination number (peak at 73.3 eV). With this assumption, 83% of Al could be in tetrahedral sites and 17% in octahedral sites on the analyzed surface of sample C. So, probably, the presence of this garnet phase in the surface of sample C has an influence on the recombination coefficient and leads to one apparent activation energy equivalent to one main recombination mechanism in all the temperature range.

### 4.3 Energy accommodation coefficient $\beta$ - mesoscopic approach

The chemical energy accommodation is an important parameter that characterizes the catalycity of a material. Following the determination of the thermal flux of recombination  $q_{rec,acc}$  transferred to the surface, an analytical expression can be proposed to deduce the chemical energy accommodation coefficient  $\beta$ .

First, it is supposed that the  $\beta$  coefficient can be represented as the ratio of the number of oxygen atoms recombined at the material surface that transfer their recombination energy to the material  $N_{O,rec}^{acc}$  to the total number of oxygen atoms recombined at the surface  $N_{O,rec}$ . Therefore, the number of oxygen atoms  $N_{O,rec}^{acc}$  is linked to the thermal flux of recombination  $q_{rec,acc}$ . Finally, the accommodation coefficient is expressed by:

$$\beta = \frac{q_{rec,acc} \cdot S_{eff} \cdot N_A}{\gamma \cdot N_{O,tot} \cdot V_O \cdot E_{rec}^{O_2}} \quad (14)$$

with  $S_{eff}$  the effective surface area,  $N_A$  the Avogadro number,  $\gamma$  the recombination coefficient,  $N_{O,tot}$  the total number of O atoms,  $V_O$  the atomic oxygen velocity,  $E_{rec}^{O_2}$  the energy of recombination to form  $O_2$  molecules.

Figures 8 and 9 present respectively the results obtained for both  $\gamma$  and  $\beta$  coefficients for  $\beta$ -cristobalite and the A sintered alumina versus temperature. Similar to experimental data obtained on metallic surfaces by Halpern [16], the  $\beta$  coefficient of cristobalite and alumina is a strong function of the surface temperature and the resulted values are very different from 1, especially at high temperature.

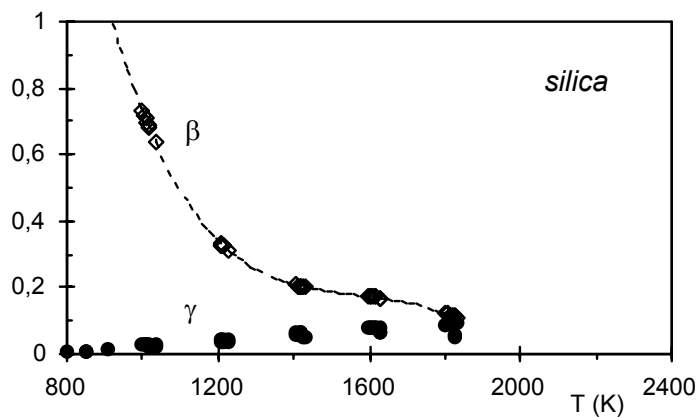
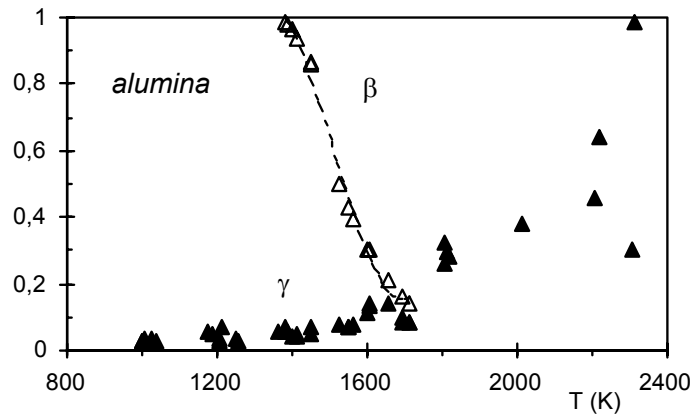


Figure 8:  $\gamma$  and  $\beta$  recombination coefficients versus temperature for cristobalite (silica)



**Figure 9:**  $\gamma$  and  $\beta$  recombination coefficients versus temperature for the A sintered alumina

This study is still in progress because, as shown in Eq. (14), the knowledge of the absolute concentration of atomic oxygen is required to increase the accuracy on the experimental results. Several techniques are now envisaged to reach this absolute concentration.

Another important point to increase also the accuracy on the measurement of the recombination parameters is the evaluation of the gas temperature profile. Some preliminary results were recently obtained by the measurement of the image of  $N_2$  bands in the plasma discharge to reach the rotational temperature of  $N_2$  in the 2<sup>nd</sup> positive system ( $C^3\Pi_u - B^3\Pi_g$ ). The comparison of experimental spectra is performed with calculated spectra to finally obtain the rotational temperature comparable to the gas temperature in such non-equilibrium plasmas. Finally, we will have, nearly at the same time, the profiles of the gas temperature and of the concentration of atomic oxygen above the surface with a spatial resolution of 270  $\mu m$ .

## 5. MOLECULAR DYNAMICS SIMULATION

In collaboration with Cacciatore, to extract more information at the atomic scale level of such heterogeneous reaction mechanisms, a semi-classical Molecular Dynamics simulation of the heterogeneous oxygen molecule formation over  $\beta$ -quartz were performed according to the E-R mechanism at a surface temperature of 1000 K during the PhD of Bedra [34] (co-tutelle Balat-Pichelin and Cacciatore).

This chapter is not detailed as Cacciatore will present the theory and results in the same conference (cf his paper). A few words on the method are just given here.

As a starting point, a 3D sample cluster is built up. Then, phonons dynamics is studied using an appropriate interatomic potential taken from literature. The collision dynamics are performed according to a semi-classical method taking into account the energy exchange processes between the surface atoms and the O and  $O_2$  particles in the gas phase. The  $O_2$  formation probability is calculated at different collisional energies of the incoming gas oxygen atoms, together with others possible reaction channels taking place at the surface. Previous MD results obtained for the recombination coefficient  $\gamma$  on  $\beta$ -cristobalite surfaces [32] were in good agreement with experiments and recently we have demonstrate the different catalytic behaviour of these two silica polymorphs. The present MD calculations are encouraging since, similarly to

the experiments, they show much smaller recombination probabilities of the oxygen atoms over quartz than for cristobalite. Unlike experimental approach, MD provides intrinsic physico-chemical properties as the vibrational state selected, the vibro-rotational energy distribution of the formed O<sub>2</sub> molecules or the exothermic energy fraction transferred to the material by heat flux that is also the definition of the accommodation coefficient  $\beta$ .

## 6. COMPARISON WITH LITERATURE DATA

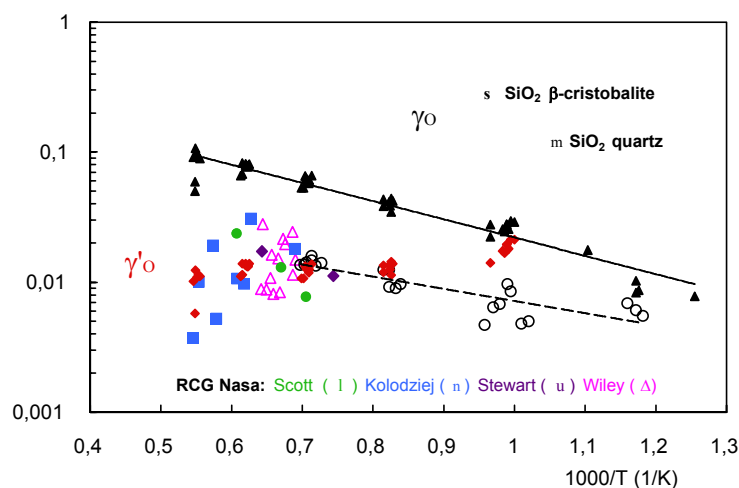
The comparison with literature data is difficult because most of the studies are realized at room temperature or at temperature higher than 1400 K but only for RCG (Reaction Cured Glass) coating (borosilicate glass with 94% silica, 4% B<sub>2</sub>O<sub>3</sub> and 2% SiB<sub>4</sub>) and, moreover, without any information on the surface morphology of the samples.

Nevertheless, our experimental results, obtained in microwave-induced air plasma, are consistent with the results of Jumper on quartz silica ( $\gamma = 14 \cdot 10^{-3}$  at 900 K) [2], of Greaves and Linnett ( $\gamma = 14 \cdot 10^{-3}$  at 873 K) [35], and of Cacciatore on  $\beta$ -cristobalite ( $\gamma = 29 \cdot 10^{-3}$  at 1000 K) [32]. Kim find lower value on quartz ( $\gamma = 29 \cdot 10^{-5}$  at 1030 K) [11] because of the low pressure used (27 Pa). The results obtained by Deutschmann [14] and Nasuti [15] modelling on silica agree both with our values, giving  $\gamma = 10^{-2}$  at 1000 K.

The RCG coating gives different values according to Rakich ( $\gamma = 5 \cdot 10^{-4}$ ) [36] or Stewart ( $\gamma = 10^{-3}$ ) [37].

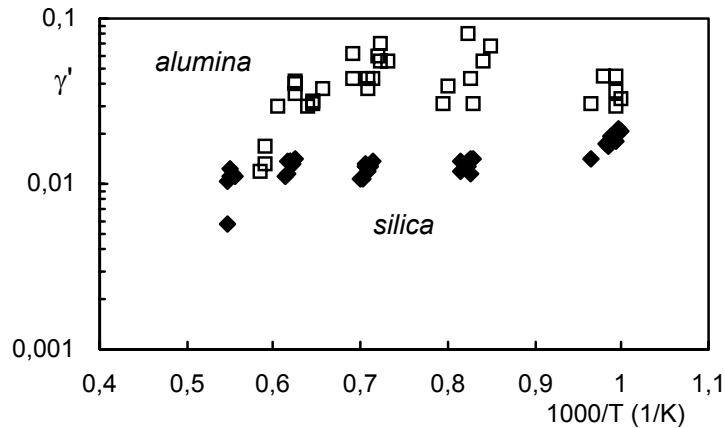
We have reported on Figure 10, in order to compare our experimental results with those obtained on arc-jet plasma facilities, the effective recombination coefficient  $\gamma'$  calculated as the product ( $\gamma \cdot \beta$ ) and that is the global recombination parameter obtained from heat flux measurements on arc-jet or plasmatron facilities.

The results obtained using actinometry and thermal flux measurements seem to be in relative good agreement with those obtained using different methods such as those used in arc-jet facilities based on the relative heating rate of a known catalytic body compared to the studied surface, taking into account the accuracy of the results and the difficulty of such measurements.



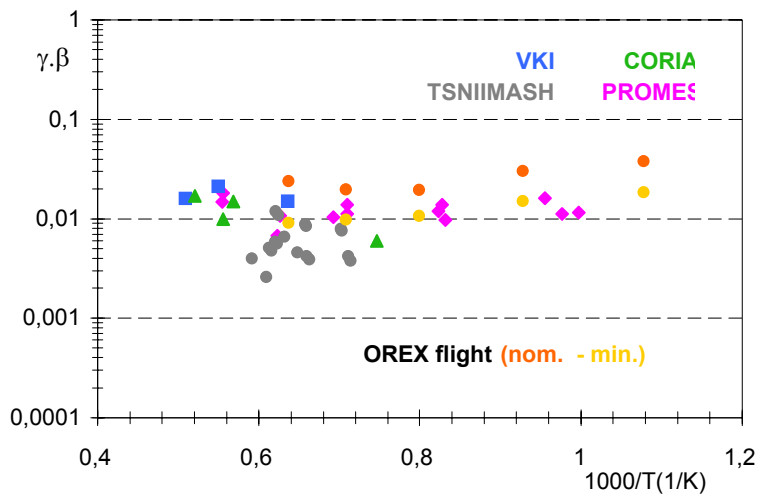
**Figure 10: Comparison of our experimental results of  $\gamma$  (on  $\beta$ -cristobalite and quartz, in black) and  $\gamma'$  (on  $\beta$ -cristobalite, in red) with those of RCG Nasa from [1, 3-5] versus reciprocal temperature**

Figure 11 represents the effective recombination obtained for silica and alumina. The effective recombination coefficient goes from 0.019 to 0.011 for  $\beta$ -cristobalite and from 0.050 to 0.012 for alumina (sample A) in the temperature range 1000-1800K with a maximum of around 0.08 at 1400 K, also showing a higher catalycity for alumina.



**Figure 11: Effective recombination coefficient  $\gamma'$  versus reciprocal temperature for  $\beta$ -cristobalite (silica) and the A sintered alumina**

Another example is given by the results obtained for OREX materials in order to compare our results with those obtained on plasmatron facilities (inductive plasma). Figure 12 presents the results of the effective recombination coefficient on carbon/carbon composites with an oxidation resistant coating. This work was done under a CNES-JAXA cooperation to compare the results obtained on ground facilities to the results obtained during the flight of the OREX re-entry capsule that was lost in the sea. On Figure 12, we report the values obtained on three inductive plasma facilities: CORIA (France), VKI (Belgium) and TSNIMASH (Russia) and compared to our results obtained on the microwave-induced plasma of the MESOX set-up (PROMES, France). The nominal and minimal values of OREX flight given by JAXA are also reported.



**Figure 12: Comparison of the effective recombination coefficient  $\gamma'$  for OREX materials versus reciprocal temperature**

The results obtained by direct (MESOX facilities) and indirect (plasmatron facilities) methods for the effective recombination coefficient  $\gamma'$  provide comparable values in all the temperature range when the recombination coefficient  $\gamma$  from actinometry measurement is multiplied by the corresponding chemical energy accommodation coefficient  $\beta$ . This normalization is necessary to have consistent data as the catalytic model in plasmatron methodology assumes an arbitrary accommodation coefficient of unity.

## 7. CONCLUSIONS

The determination of the atomic oxygen recombination at the surface of different sintered ceramic materials at high temperature under low air pressure plasma has been realized in the MESOX set-up using a multi-scale approach.

At the mesoscopic scale, the thermal method is based on a heat balance on materials under air and argon plasmas. This approach leads to the determination of the temperature increase due to the catalytic recombination of atomic oxygen and to the evaluation of the thermal flux of recombination transferred to the surface. A low influence of the pressure has been observed between 200 and 2000 Pa air, that can come from a limitation of the recombination by the number of active sites and the prevalence of the Eley-Rideal mechanism, with recombination reactions between an atom in the gaseous phase and one adsorbed, this being in accordance with literature results. The temperature increase is more pronounced at low temperature level and decreases rapidly with surface temperature. Thermal fluxes of recombination have also been calculated from heat balance with a one-dimensional hypothesis. Catalytic activities for the different materials move weakly between 1000-1400 K, except for  $\text{Al}_2\text{O}_3$  for which recombination fluxes vary strongly and reach a maximum at 1400 K. Most of the studied materials are weakly catalytic (except  $\text{Al}_2\text{O}_3$ ) and were classified according to a catalytic scale available between 1000 and 1800 K:  $\text{SiC} \approx \text{SiC} + \text{SiO}_2 \leq \text{Si}_3\text{N}_4 \leq \text{AlN} \approx \text{AlN} + \text{Al}_2\text{O}_3 \ll \text{Al}_2\text{O}_3$ .

A heat transfer modelling at high temperature has been developed in order to identify the absorbed microwave flux and finally the thermal flux of recombination and, also, to precise the validity of the experimental assumptions. The catalytic scale is confirmed by using the bi-dimensional modelling and give more accurate values of the thermal flux of recombination particularly for temperatures lower than

1400 K; the discrepancy between modelling and experimental values of the thermal flux of recombination being less important at higher temperature levels (1600 - 1800 K).

At the same scale, the evaluation of the chemical energy accommodation coefficient  $\beta$  has been carried out to obtain all the parameters describing the atoms recombination on surfaces. Moreover, the measurement of this coefficient lets possible the comparison with high enthalpy facilities (arc-jet and plasmatron).

At the microscopic level, new experimental results were obtained on the recombination coefficient of atomic oxygen  $\gamma$  at the surface of ceramic materials at high temperature using relative atomic concentration measurements (chemical approach). This work has followed the evaluation of the thermal flux of recombination  $q_{\text{rec,acc}}$  transferred to the surface material in the same temperature range. Experimental results have shown the importance of the crystalline lattice (silica polymorphs) and of the impurity content (polycrystalline  $\alpha$ -alumina) on the recombination coefficient.

At the atomic scale, the study done in collaboration with Cacciatore by Molecular Dynamics simulation has given first interesting results not only on the recombination coefficient but also on the several energy transfers in the formed oxygen molecule leaving the surface after recombination of oxygen atoms.

Both these data  $\gamma$  and  $\beta$  are very useful for the calculation and design of the planetary entry of hypersonic vehicles and for comparison with results obtained by indirect methods on arc-jet or plasmatron facilities.

## **8. REFERENCES**

- [1] Scott C.D., AIAA Paper 80-1477, July 1980.
- [2] Jumper, E.J., Seward W.A., J. Thermophys. & Heat Transfer, 8 (3), 1994, 460-465.
- [3] Kolodziej P., Stewart D.A., AIAA Paper 87-1637, June 1987.
- [4] Willey R.J., J. Thermophys. & Heat Transfer, 7 (1), 1993, 55-62.
- [5] Stewart D.A., Rakich J.V., Lanfranco M.J., NASA CP-2283, Part 2, March 1983, 827-845.
- [6] Zoby E.V., Gupta R.N., Simmonds A.L., Progr. Astron. Aeron., 96, 1985, 445-464.
- [7] Clark R.K., Cunnington G.R., Wiedemann K.E., J. Spacecrafts & Rockets, 32 (1), 1995, 89-96.
- [8] Cunnington G., Robinson J., Clark R., AIAA Paper 90-1742, June 1990.
- [9] Vasil'evskii S.A., Kolesnikov A.F., Yakushin M.I., High Temp., 1991, 411-418.
- [10] Gordeev A.N., Kolesnikov A.F., Yakushin M.I., SAMPE J., 28 (3), 1992, 29-33.
- [11] Kim Y.C., Boudart M., Langmuir, 7, 1991, 2999-3005.
- [12] Pallix J.B., Copeland R.A., J. Thermophysics & Heat Transfer, 10 (2), 1996, 224-233.
- [13] N'Guyen-Xuan F., Hassouni K., Cavadias S., Amouroux J., Proceed. 11<sup>th</sup> Int. Symp. Plasma Chem., Loughborough (UK), 4, 1993, 1516-1521.
- [14] Deutschmann D., Riedel U., Warnatz J., J. Heat Transfer, 117, 1995, 495-501.

- [15] Nasuti F., Barbato M., Bruno C., *J. Thermophys. & Heat Transfer*, 10 (1), 1996, 131-136.
- [16] Halpern B., Rosner D.E., *Trans. Faraday Soc.*, 74 (8), 1978, 1883-1912.
- [17] Melin G.A., Madix R.J., *Trans. Faraday Soc.*, 67, 1971, 198-211
- [18] Carleton K.L., Marinelli W.J., *J. Thermophysics & Heat Transfer*, 6 (4), 1992, 650-655.
- [19] Clark R.K., Cunnington G.R., Robinson J.C., *J. Thermophysics*, 1 (1), 1987, 28-34.
- [20] Daiss A., Frühauf H.H., Messerschmid E.W., *AIAA Paper 96-1903*, June 1996.
- [21] Balat-Pichelin M., Robert J.F., Sans J.L., *Appl. Surf. Sci.*, under press, 2006.
- [22] Balat M., *J. Eur. Ceram. Soc.*, 16, 1996, 55-62.
- [23] Balat-Pichelin M., Duqueroie F., *Int. J. Thermal Sci.*, 40, 2001, 279-287.
- [24] Balat-Pichelin M., Badie J.M., Berjoan R., Boubert P., *Chem. Phys.* 291, 2003, 181-194.
- [25] Granier A., Chéreau D., Henda K., Safari R., Leprince P., *J. Appl. Phys.*, 75 (1), 1994, 104-114.
- [26] Booth J.P., Joubert O., Pelletier J., Sadeghi N., *J. Appl. Phys.*, 69 (2), 1991, 618-626.
- [27] Diamy A.M., Legrand J.C., Al Andari J., *New. J. Chem.* 21, 1997, 177-185.
- [28] Walkup R.E., Saenger K.L., Selwyn G.S., *J. Chem. Phys.*, 84, 1996, 2668-2674.
- [29] Balat-Pichelin M., Badie J.M., Cacciatore M., Rutigliano M., 4<sup>th</sup> Eur. Work. Hot Structures and Thermal Protection Systems for Space Vehicles Palermo (Italy), ESA SP-521, April 2003, 403-410.
- [30] Bedra L., Balat-Pichelin M., Rutigliano M., Cacciatore M., *Rarefied Gas Dynamics*, AIP Conf. Proceed Subseries Atomic, Molecular & Chemical Physics, Ed. M. Capitelli, 762, May 2005, 1037-1042.
- [31] Bedra L., Rutigliano M., Cacciatore M., Balat-Pichelin M., to be published in *Langmuir*, 2006.
- [32] Cacciatore M., Rutigliano M., Billing G.D., *J. Themophys. & Heat Transfer* 13, 1999, 195-203.
- [33] Guerra V., *Rarefied Gas Dynamics*, AIP Conf. Proceed Subseries Atomic, Molecular & Chemical Physics, Ed. M. Capitelli, 762, May 2005, 981-986.
- [34] Bedra L., PhD thesis, Perpignan University, 27 June 2005.
- [35] Greaves J.C., Linnett J.W., *Trans. Faraday Soc.*, 55, 1959, 1355-1361.
- [36] Rakich J.V., Stewart D.A., Lanfranco M.J., *Progr. Astron. & Aeron.* 85, 1983, 97-122.
- [37] Stewart D.A., Rakich J.V., Lanfranco M.J., *NASA CP-2283*, Part 2, 1983, 827-845.

## ACKNOWLEDGEMENTS

The author wants to thank for their fruitful collaboration her colleagues, particularly J.M. Badie and R. Berjoan, and PhD students from PROMES-CNRS laboratory and from outside P. Boubert (IUSTI Marseille), M. Cacciatore and M. Rutigliano (IMIP-CNR Bari), O. Gerasimova for AFM (USU, Ekaterinburg), A. Enzian (CNES, Paris), M. Mozetic and A. Vesel (JSI, Ljubljana).

## NOMENCLATURE

C	concentration, atom/m <sup>3</sup>
D	binary diffusion coefficient, m <sup>2</sup> /s
E <sub>a</sub>	apparent activation energy, kJ/mol
E-R	Eley-Rideal
I	intensity (a.u)
k <sub>B</sub>	Boltzmann constant
k <sub>w</sub>	catalytic recombination rate, m/s
L	thickness of the boundary layer, m
L-H	Langmuir-Hinshelwood
M	molar mass, g/mol
N	number of atoms
N <sub>A</sub>	Avogadro number
P	total pressure, Pa
q	thermal flux, W/m <sup>2</sup>
r	radius, m
S	area, m <sup>2</sup>
t	time, s
T	temperature, K
U	mass transfer velocity, m/s
V	mean square atomic velocity, m/s
x	abscissa, m

### *Greek letters*

α	solar absorptivity coefficient
β	chemical energy accommodation coefficient
ΔT	difference between two temperatures, K
ε	total hemispherical emissivity
γ	recombination coefficient
λ	wavelength, μm
ω	variation of concentration
σ	Stefan-Boltzmann constant

### *Subscripts*

acc	accommodation
Ar	argon
b	back face of the sample
eff	effective
f	front face of the sample
g	gas
lat	lateral thermal losses at the limit of the reference cylinder
mw	microwave (microwave-material interaction)
0	zero (at x=0)

O	atomic oxygen
rad	radiative transfer
rec	recombination
s	surface
sol	solar
tot	total

*Superscripts*

air	under air flow
arg	under argon flow
*	under plasma conditions

